Optimal Pilot Sequences for Phase and Timing Synchronization in FTN Systems

Leila Mounsif, Damien Roque, Charly Poulliat

Optimal Pilot Sequences for Phase and Timing Synchronization in FTN Systems

Leila Mounsif*†, Damien Roque* and Charly Poulliat†
*ISAE-SUPAERO, Université de Toulouse, France
Email: {leila.mounsif,damien.roque}@isae-supaero.fr
†INPT/ENSEEIHT, Université de Toulouse, France
Email: {leila.mounsif,charly.poulliat@enseeiht.fr}

***Abstract*—In this paper, we study the joint phase and timing estimation problem in Faster-than-Nyquist (FTN) systems. We use the Cramér–Rao lower bound (CRB) as a cost function to design optimal pilot sequences subject to an energy constraint. We rely on harmonic approximations of the bound to establish closed-form relations between the ultimate synchronization performance and the transmitted waveform characteristics (*i.e.*, pulse shaping filter and signaling density). We show that increasing the symbol rate at fixed bandwidth is beneficial to phase estimation and detrimental to timing synchronization. Therefore, we propose a joint timing/phase pilot design to accommodate this trade-off. Lastly, we illustrate the strengths of the proposed pilots with respect to traditional Zadoff–Chu sequences in presence of a residual carrier frequency offset.**

I. Introduction

A single-carrier linearly modulated signal is said *Faster-than-Nyquist* (FTN) iff the symbol rate is greater than the transmit pulse's bandwidth [1]. This transmission strategy is promising to increase spectral efficiency at fixed constellation size, especially in power-constrained channels (*e.g.* mobile and satellite communications, optical fiber) [2]–[5]. Additionally, FTN signals exhibit low-probability of intercept (LPI) properties: (i) their cyclic autocorrelation function vanishes at multiples of the symbol rate [6]; (ii) filter-hopping techniques and time-varying symbol rate are new degrees of freedom to support physical layer security [7], [8].

However, FTN signaling comes at the cost of intersymbol-interference (ISI) which requires advanced precoding and/or detection schemes to take advantage of the underlying spectral efficiency gain at an acceptable error probability (*e.g.*, [9]–[11]). Most of these contributions assume a perfectly synchronized receiver, eluding the unexplored timing, phase and frequency estimation problem in presence of non-orthogonal pulse shapes. In the following, we focus on pilot-aided (PA) synchronization with time-invariant parameters.

A trivial approach consists in sending pilots at the Nyquist rate prior to an FTN data transmission. Those two sequences are possibly separated by a time gap to avoid interpulse interference. In this case, one may reuse traditional Nyquist-rate synchronization techniques: the so-called *zero-one alternating* pilot sequence is shown to achieve satisfactory results in terms of Cramér–Rao lower bound (CRB) for joint timing and phase estimation [12] and practical maximum-likelihood (ML)-based estimators can be subsequently derived [13].

However, a more challenging and bandwidth-efficient strategy relies on a fully FTN transmission (*i.e.*, pilots and data symbols are transmitted at the same FTN rate). In [14], CRB-optimal (or near-optimal) timing pilots are derived as a function of the signaling density (*i.e.*, pulse compression factor). However, this work does not consider phase nor frequency offsets.

In this paper we extend [14] to the design of joint phase/timing optimal pilots in FTN scenarios. Our contribution may also be seen as a follow-up to [15] *via* a generalization to non-orthogonal pulses. We show that phase and timing CRB-optimal pilot sequences both accept closed-form asymptotic approximations. In particular, we build a real-valued orthogonal basis where each vector corresponds to an optimal timing or phase pilot at a given signaling density. As in [15], the restriction to real-valued pilot sequences conveniently decouples the two parameters of interest. We reveal a timing/phase estimation trade-off: as the signaling density increases, the former parameter's estimation is penalized while it is beneficial to the latter. Therefore, we propose a joint timing/phase pilot design efficiently implemented by reusing the aforementioned CRB approximation.

The rest of this paper is organized as follows. In Section II we define the observation model: linearly modulated pilots are transmitted over an additive white Gaussian noise (AWGN) channel in presence of timing, phase and frequency offsets. Then we recall the expression of timing and phase CRBs assuming a pre-compensated frequency offset. In Section III, we derive closed-form approximations of the bounds to reveal the impact of underlying pulse shape and signaling density. We determine optimal timing/phase pilot sequences accordingly and we illustrate their performance in Nyquist and FTN scenarios based on root-raised cosine (RRC) pulses. In Section IV, we study the robustness of the proposed CRB-optimal sequences in presence of residual frequency offset; to this extent we specify ML-based timing and phase estimators. We also benchmark the proposed CRB-optimal pilots against traditional Zadoff–Chu (ZC) root sequences [16]. Finally, Section V draws our conclusions.

Notation: $\mathbf{Z}$ and $\mathbf{R}$ are the sets of integer and real numbers, respectively. $\mathcal{I}_N$ is the finite set $\{0,\dots,N-1\}$. We use $\cdot^{\mathsf{T}}$

The work of Leila Mounsif is supported by AID under grant 2018.60.0014.

to denote transpose, $\cdot^*$ conjugate and $\cdot^{\mathsf{H}}$ conjugate transpose. $\mathcal{E}\{\cdot\}$ is the expectation operator. $\|\cdot\|_2$ is the Euclidean norm for continuous-time or discrete-time signals, depending on the context.

II. Observation model with timing, phase and frequency offsets

A. System model

We consider a single-carrier linear modulation, observed in presence of timing, phase and frequency synchronization impairments denoted ξ, ϕ, F, respectively:

$$r_{\mathrm{c}}(t) \triangleq e^{j(2\pi Ft+\phi)} \sum_{k\in\mathcal{I}_K} c_k g(t-kT_s-\xi T_s) + w_{\mathrm{c}}(t),\ t\in\mathbf{R} \tag{1}$$

where $\{c_k\}_{k\in\mathcal{I}_K}$ represents a pilot sequence (*i.e.*, pattern known by the receiver), $g(t)$ is a real-valued pulse shaping filter characterized by a frequency support $(-B/2; B/2)$ and enforcing $\|g\|_2^2 = 1$, T_s is the symbol period and $w_{\mathrm{c}}(t)$ is a white noise with power spectral density $2N_0$.

The signaling density is defined as $\rho \triangleq 1/(BT_s)$ and a transmission is reputed to be FTN iff $\rho > 1$ [1].

We sample (1) after an ideal low-pass filter $v(t) \triangleq 1/T\,\mathrm{sinc}(t/T)$ for notational convenience[1]. The sampling rate $1/T$ is chosen such that $1/T \geq B + F_{\max}$ with $F_{\max}$ the greatest possible frequency offset (*i.e.*, $|F| \leq F_{\max}$):

$$\begin{aligned} r(nT) &\triangleq (r_{\mathrm{c}} * v)(nT) \\ &= e^{j(2\pi\nu n+\phi)} \sum_{k\in\mathcal{I}_K} c_k g(nT-kT_s-\xi T_s) \\ &\quad + w(nT), \quad n\in\mathbf{Z} \end{aligned} \tag{2}$$

where $\nu \triangleq FT$ is the normalized frequency offset and $w(nT) \triangleq (w_{\mathrm{c}} * v)(nT)$ are uncorrelated noise samples.

In practice, the impulse response $g(t)$ is truncated to N_g symbol periods; this number is selected large enough to reasonably preserve the bandlimited assumption. Without loss of generality T_s/T is chosen as a positive integer such that $N \triangleq T_s(N_g+K)/T$ denotes the number of "useful" samples to be captured from (2). Those samples are gathered in $\boldsymbol{r} \triangleq [r(-(N/2)T)\, r((-N/2+1)T) \dots r((N/2-1)T)]^{\mathsf{T}}$, compactly expressed by

$$\boldsymbol{r} = e^{j\phi}\boldsymbol{D}_\nu \boldsymbol{G}_\xi \boldsymbol{c} + \boldsymbol{w} \tag{3}$$

where

- $\boldsymbol{G}_\xi$ is the shaping matrix with entries $[\boldsymbol{G}_\xi]_{n,k} = g(nT - kT_s - \xi T_s)$, $k\in\mathcal{I}_K$, $n\in\{-N/2\, -N/2+1 \cdots N/2-1\}$;
- $\boldsymbol{D}_\nu$ is an $(N\times N)$ diagonal matrix, with $[\boldsymbol{D}_\nu]_{m,m} = e^{j2\pi\nu(m-N/2)}$, $m\in\mathcal{I}_N$ associating a regular phase shift to each sample;
- $\boldsymbol{c} = [c_0 \dots c_{K-1}]^{\mathsf{T}}$ is the pilot sequence vector;
- $\boldsymbol{w} = [w(-(N/2)T)\, w((-N/2+1)T) \dots w((N/2-1)T)]^{\mathsf{T}}$ is the noise vector such that $\boldsymbol{w} \sim \mathcal{CN}(\boldsymbol{0}, \sigma_w^2 \boldsymbol{I}_N)$, where σ_w^2 is related to the per-symbol energy E_s for independent and uniformly distributed (iud) symbols by $\sigma_w^2 \triangleq T^{-1}(E_s/N_0)^{-1}$.

To exemplify the upcoming results, Tab. I summarizes the default values of the aforementioned parameters.

TABLE I
Default simulation settings

Parameter	**Value**
Filter type	RRC
Roll-off factor α	0.2
Impulse response truncation length N_g	64
Pilot sequence length K	50 symbols
Signal-to-noise ratio E_s/N_0	10 dB
Number of samples per symbol T_s/T	4

B. Timing and phase CRBs in the pilot-aided case

Although we study the impact of a residual carrier frequency offset in Section IV (*i.e.*, $\nu \neq 0$), we first establish the *Fisher information matrix* (FIM) for phase and timing unknown parameters only:

$$\boldsymbol{J} = \begin{bmatrix} J_{\xi,\xi} & J_{\xi,\phi} \\ J_{\phi,\xi} & J_{\phi,\phi} \end{bmatrix} \tag{4}$$

where each element is directly obtained from [18, Eq. (15.52)]:

$$J_{\xi,\xi} = \frac{2}{\sigma_w^2} \boldsymbol{c}^{\mathsf{H}} \dot{\boldsymbol{G}}_\xi^{\mathsf{H}} \dot{\boldsymbol{G}}_\xi \boldsymbol{c}, \tag{5}$$

$$J_{\phi,\phi} = \frac{2}{\sigma_w^2} \boldsymbol{c}^{\mathsf{H}} \boldsymbol{G}_\xi^{\mathsf{H}} \boldsymbol{G}_\xi \boldsymbol{c}, \tag{6}$$

$$J_{\xi,\phi} = J_{\phi,\xi} = \frac{2}{\sigma_w^2} \Re\left\{ j\boldsymbol{c}^{\mathsf{H}} \dot{\boldsymbol{G}}_\xi^{\mathsf{H}} \boldsymbol{G}_\xi \boldsymbol{c} \right\} \tag{7}$$

with $\dot{\boldsymbol{G}}_\xi \triangleq \mathrm{d}\boldsymbol{G}_\xi/\mathrm{d}\xi$. From (4) the general expression of the CRB is

$$\mathrm{CRB}(\psi_i|\boldsymbol{c}) \triangleq \frac{J_{\psi_j,\psi_j}}{J_{\phi,\phi}J_{\xi,\xi} - J_{\xi,\phi}^2}, \quad \psi_i,\psi_j \in \{\xi,\phi\} : \psi_i \neq \psi_j. \tag{8}$$

From (8), it is clear that $J_{\xi,\phi}$ is wanted as small as possible. In particular, if $\boldsymbol{c}$ is real-valued, then $J_{\xi,\phi} = J_{\phi,\xi} = 0$, as shown in [15, Lemma 3]. We restrict our study to this case in the following since it conveniently decouples ξ and ϕ, thereby enabling a separate estimation approach:

$$\mathrm{CRB}(\psi|\boldsymbol{c}) = \left(\frac{2}{\sigma_w^2} \boldsymbol{c}^{\mathsf{H}} \boldsymbol{P}_\psi \boldsymbol{c} \right)^{-1}, \quad \psi \in \{\xi,\phi\} \tag{9}$$

with $\boldsymbol{P}_\xi = \dot{\boldsymbol{G}}_\xi^{\mathsf{H}} \dot{\boldsymbol{G}}_\xi$ and $\boldsymbol{P}_\phi = \boldsymbol{G}_\xi^{\mathsf{H}} \boldsymbol{G}_\xi$.

Besides having a Toeplitz structure, both matrices $\boldsymbol{P}_\xi$ and $\boldsymbol{P}_\phi$ are banded if we assume a greater pilot length K than

[1]More realistic T-orthogonal filters with some excess bandwidth are acceptable to yield white noise samples while preserving a sufficient statistic for synchronization and symbol detection [17].

autocorrelation supports for $\mathrm{d}g(nT)/\mathrm{d}\xi$ and $g(nT)$, respectively. Therefore a circulant approximation can suitably be applied to $\boldsymbol{P}_\psi$, motivating the following asymptotic spectral decomposition [19]:

$$\boldsymbol{P}_\psi \overset{K\gg 1}{\approx} \boldsymbol{F}_K^{\mathsf{H}} \tilde{\boldsymbol{\Lambda}}_\psi \boldsymbol{F}_K \tag{10}$$

where $\boldsymbol{F}_K$ is the unitary discrete Fourier transform (DFT) matrix whose columns are denoted $\{\boldsymbol{f}_k\}_{k\in\mathcal{I}_K}$ and $\tilde{\boldsymbol{\Lambda}}_\psi = \mathrm{diag}\left\{\tilde{\lambda}_{\psi,1}, \tilde{\lambda}_{\psi,2} \dots \tilde{\lambda}_{\psi,K-1}\right\}$ gathers the corresponding eigenvalues:

$$\tilde{\lambda}_{\psi,k} = \sqrt{K}\left[\boldsymbol{F}_K \boldsymbol{p}_{\psi,\mathrm{c}}\right]_k, \quad k \in \mathcal{I}_K \tag{11}$$

with $\boldsymbol{p}_{\psi,\mathrm{c}}$ the "circularized" first column of $\boldsymbol{P}_\psi$.

III. Design of Joint Timing and Phase Optimal Pilot Sequences

A. Real-valued optimal timing or phase pilot sequences

We first derive CRB-optimal timing and phase pilot sequence based on (9)-(11) subject to energy and real value constraints.

Since $g(t)$ is real-valued, $\tilde{\lambda}_{\psi,k}$ and $\tilde{\lambda}_{\psi,K-k}$ are equal; their corresponding eigenvectors are $\boldsymbol{f}_k$ and $\boldsymbol{f}_k^*$. As a consequence, the unitary DFT basis in (10) may be replaced by a (real) orthogonal basis denoted $\tilde{\boldsymbol{F}}_K^{\mathsf{T}}$ where the columns $\tilde{\boldsymbol{f}}_k$ are built as follows:

$$\tilde{\boldsymbol{f}}_k = \begin{cases} \boldsymbol{f}_k & \text{if } \boldsymbol{f}_k \text{ is real-valued} \\ \sqrt{2}\Re\{\boldsymbol{f}_k\} & \text{if } \boldsymbol{f}_k \text{ is complex-valued and } k \le \lfloor \frac{K}{2} \rfloor, \\ \sqrt{2}\Im\{\boldsymbol{f}_k\} & \text{if } \boldsymbol{f}_k \text{ is complex-valued and } k > \lfloor \frac{K}{2} \rfloor. \end{cases} \tag{12}$$

We first take $\mathrm{CRB}(\psi|\boldsymbol{c})$ as a cost function for the design of real-valued optimal pilot sequences. Using (9), (10) and (12), the optimization problem becomes

$$\begin{aligned} \tilde{\boldsymbol{c}}_{\psi,\mathrm{opt}} = \arg\max_{\boldsymbol{c}} & \boldsymbol{c}^{\mathsf{T}} \tilde{\boldsymbol{F}}_K^{\mathsf{T}} \tilde{\boldsymbol{\Lambda}}_\psi \tilde{\boldsymbol{F}}_K \boldsymbol{c} \\ \text{s.t. } & \|\boldsymbol{c}\|_2^2 = K. \end{aligned} \tag{13}$$

Considering the quadratic form in (13), the solution is directly obtained *via* the *maximum principle* [20, Th. 6.5]:

$$\tilde{\boldsymbol{c}}_{\psi,\mathrm{opt}} = \sqrt{K}\tilde{\boldsymbol{f}}_{k_{\max}} \tag{14}$$

where $k_{\max}$ refers to the index of the largest $|\tilde{\lambda}_{\psi,k}|$, $k \in \mathcal{I}_K$.

In [14, Th. 1] a closed-form approximation of $\{\tilde{\lambda}_{\xi,k}\}_{k\in\mathcal{I}_K}$ is provided for long pilot sequences. Herein, we focus on the case where $\rho \ge 1/2$ since the filters specified in Tab. I are such that $\alpha \le 1$. We perform similar derivations to encompass phase and timing parameters:

$$\tilde{\lambda}_{\psi,k} \overset{K\gg 1}{\approx} \frac{1}{T_s T}\left[H_\psi\left(\rho B \frac{k}{K}\right) + H_\psi\left(\rho B \frac{K-k}{K}\right)\right] \tag{15}$$

with $H_\xi(f) \triangleq (2\pi T_s)^2 f^2 |G(f)|^2$, $H_\phi(f) \triangleq |G(f)|^2$ and $G(f) \triangleq \int_{-\infty}^{\infty} g(t) e^{-j2\pi ft}\mathrm{d}t$ such that $G(f) \neq 0$ for $f \in (-B/2; B/2)$.

For long-enough pilot sequences, this result exhibits a straightforward relation between the signaling density ρ and the transmit pulse's frequency response $G(f)$. In this case, the nullity of $\boldsymbol{P}_\psi$ necessarily increases with ρ in an FTN scenario (*i.e.*, $\rho > 1$). This fact is exemplified in Fig. 1 where the $\tilde{\lambda}_{\psi,k}$'s amplitude is depicted for several signaling densities. The approximation (15) turns out to be relevant even at moderate pilots lengths. At a given FTN density, there exists a single optimal timing sequence [14] while several optimal phase sequences reach the same asymptotic performance. Traditional Nyquist systems stand as a particular case where optimal timing/phase sequences are independent of the signaling density ($\rho \le 1$) [15].

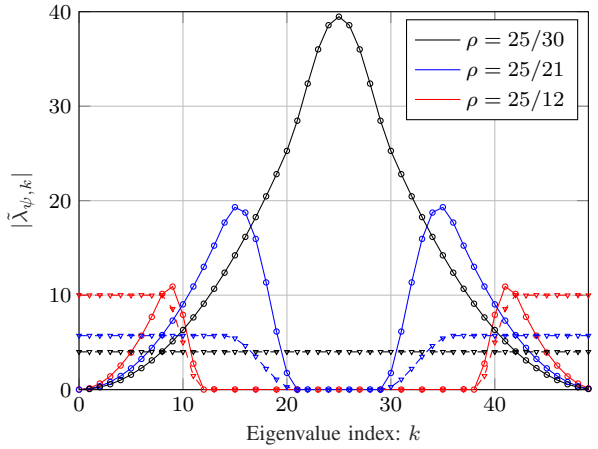

Fig. 1. Amplitude of eigenvalues $\{\tilde{\lambda}_{\xi,k}\}_{k\in\mathcal{I}_K}$ (solid lines) and $\{\tilde{\lambda}_{\phi,k}\}_{k\in\mathcal{I}_K}$ (dashed lines). The approximation in (15) is also displayed (circle and triangle marks). Several transmission densities are considered: $\rho = 25/30$ (Nyquist) and $\rho \in \{25/21, 25/12\}$ (FTN). All other parameters are set as in Tab. I.

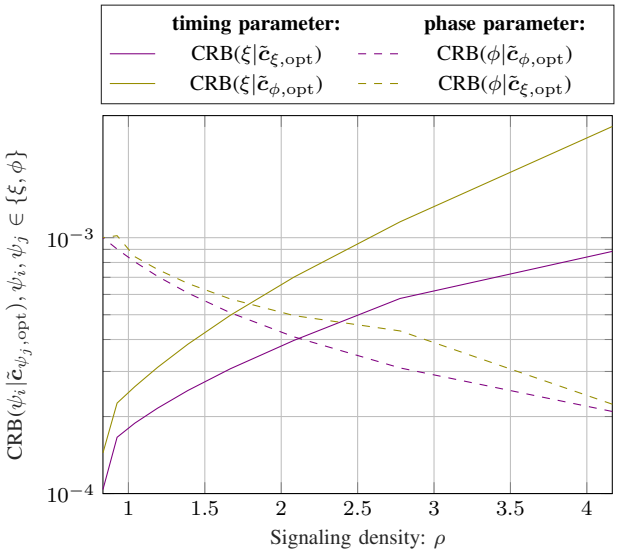

Fig. 2. $\mathrm{CRB}(\xi|\tilde{\boldsymbol{c}}_{\psi,\mathrm{opt}})$ (solid lines) and $\mathrm{CRB}(\phi|\tilde{\boldsymbol{c}}_{\psi,\mathrm{opt}})$ (dashed lines) as function of the signaling density ρ. For each CRB, the pilot sequence $\tilde{\boldsymbol{c}}_{\psi,\mathrm{opt}}$ in (14) is optimized according to both the parameter of interest (violet) and its counterpart (olive). All other values are set as in Tab. I.

In Fig. 2, we evaluate $\mathrm{CRB}(\psi_i|\tilde{\boldsymbol{c}}_{\psi_j,\mathrm{opt}})$ with $\psi_i, \psi_j \in \{\xi, \phi\}$

as a function of the signaling density ρ. $\mathrm{CRB}(\xi|\tilde{\boldsymbol{c}}_{\psi,\mathrm{opt}})$ strictly decreases with ρ [14] whereas the opposite behavior is observed for $\mathrm{CRB}(\phi|\tilde{\boldsymbol{c}}_{\psi,\mathrm{opt}})$. Among the two parameters of interest, timing estimation is the most sensitive to a suboptimal pilot sequence selection, as already hinted at in Fig. 1. In an FTN scenario, the timing/phase optimization trade-off revealed in Fig. 2 either suggests (i) the use of separate pilots for each parameter or (ii) a joint timing/phase design as proposed hereafter.

B. Timing and phase optimization trade-off

To control the timing/phase pilot optimization trade-off, we introduce a user-defined parameter $\gamma \in [0,1]$ and we define the following cost function based on the individual timing and phase CRBs in (9):

$$\mathrm{C}(\gamma,\boldsymbol{c}) = \left[\frac{2}{\sigma_w^2}\left(\gamma \boldsymbol{c}^{\mathsf{H}}\boldsymbol{P}_\xi \boldsymbol{c} + (1-\gamma)\boldsymbol{c}^{\mathsf{H}}\boldsymbol{P}_\phi \boldsymbol{c}\right)\right]^{-1}. \tag{16}$$

Owing to the approximate eigenstructure of $\boldsymbol{P}_\psi$ in (10)-(11) and its real basis expansion in (12), we specify the following joint optimization problem from (16):

$$\begin{aligned}\tilde{\boldsymbol{c}}_{\mathrm{opt}}^{\gamma} = \arg\max_{\boldsymbol{c}} \gamma \boldsymbol{c}^{\mathsf{T}}\boldsymbol{P}_\xi \boldsymbol{c} + (1-\gamma)\boldsymbol{c}^{\mathsf{T}}\boldsymbol{P}_\phi \boldsymbol{c} \\ \text{s.t. } \boldsymbol{c} \in \{\sqrt{K}\tilde{\boldsymbol{f}}_k\}_{k\in\mathcal{I}_K}.\end{aligned} \tag{17}$$

We first emphasize the low computational complexity of the maximum search in (17): for a given value of γ, the cost function in (16) is only evaluated K times. Fig. 3 depicts $\mathrm{C}(\gamma,\tilde{\boldsymbol{c}}_{\mathrm{opt}}^{\gamma})$ as a function of γ along with its asymptotic CRBs. In FTN scenarios, we observe a decreasing dynamic range of $\mathrm{C}(\gamma,\tilde{\boldsymbol{c}}_{\mathrm{opt}}^{\gamma})$ with ρ. For example, in the case where $\rho = 25/12$, the parameter γ operates a choice between only two pilot sequences. Such a restriction can be explained by the increasing nullity of $\boldsymbol{F}_K^{\mathsf{H}}\tilde{\boldsymbol{\Lambda}}_\psi \boldsymbol{F}_K$ with ρ, as asymptotically reported in (15) and illustrated with Fig. 1.

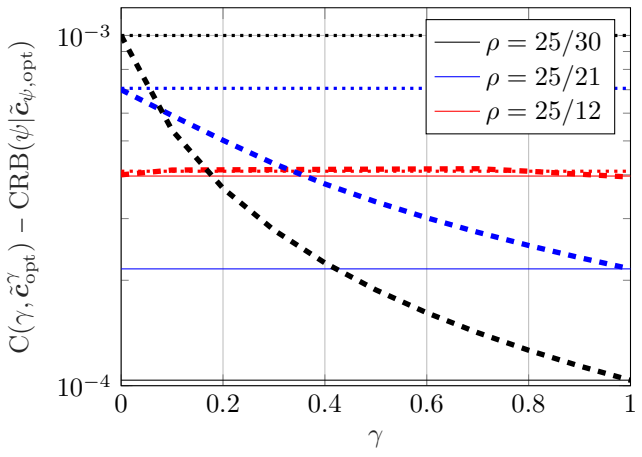

Fig. 3. Timing/phase cost function $\mathrm{C}(\gamma,\tilde{\boldsymbol{c}}_{\mathrm{opt}}^{\gamma})$ (thick dashed lines) as a function of $\gamma \in [0;1]$ and $\mathrm{CRB}(\psi|\tilde{\boldsymbol{c}}_{\psi,\mathrm{opt}})$ (solid lines for $\psi = \xi$ and dotted lines for $\psi = \phi$) as a reference. Several transmission densities are considered: $\rho = 25/30$ (Nyquist) and $\rho \in \{25/21, 25/12\}$ (FTN). All other parameters are set as in Tab. I.

IV. Maximum likelihood estimation in presence of residual frequency offset

In this Section, we evaluate the performance of the proposed timing/phase pilot sequences with the help of ML-based estimators denoted $\hat{\psi}_{\mathrm{ML}}(\boldsymbol{c})$ where $\boldsymbol{c}$ represents the pilot sequence under test. In particular, we rely on ML's *asymptotic efficiency* to assess the CRBs' "achievability" [18, Ch. 7]: in presence of orthogonal parameters ξ and ϕ we expect

$$\hat{\psi}_{\mathrm{ML}}(\boldsymbol{c}) \overset{\mathrm{a}}{\sim} \mathcal{N}(\psi, \mathrm{CRB}\left(\psi|\boldsymbol{c}\right)) \tag{18}$$

where $\overset{\mathrm{a}}{\sim}$ refers to an asymptotic distribution obtained for K large enough.

In practice, the ML estimators are implemented *via* the *golden section search* (GSS) algorithm [21] instead of a naive grid-search or a cross-correlation-based approach. In brief, the GSS algorithm performs a dichotomic-like search on the cost function, where the intervals are ruled by the golden ratio. A stop criterion in terms of step tolerance is set according to the target CRB. Since the likelihood function must be concave over the entire search interval, we limit the GSS to fine timing/phase estimation: $\xi \in [0;1)$ and $\phi \in [0;2\pi)$. The performance of $\hat{\psi}_{\mathrm{ML}}(\boldsymbol{c})$ is measured in terms of mean-squared-error: $\mathrm{MSE}(\hat{\psi}_{\mathrm{ML}}(\boldsymbol{c})) \triangleq \mathcal{E}\left\{|\hat{\psi}_{\mathrm{ML}}(\boldsymbol{c}) - \psi|^2\right\}$, through Monte Carlo simulation (10 000 random experiments).

As a baseline, we also consider the so-called Zadoff–Chu (ZC) root sequences [16] which are notably used in cellular network (*e.g.*, LTE) in virtue of their good correlation and constant amplitude properties. That said, ZC sequences have a limited practical interest in FTN scenarios because their orthogonality feature cannot be exploited directly at the symbol level due to intersymbol interference. Each ZC root sequence is denoted $\boldsymbol{c}_{\mathrm{ZC}}^{p} \triangleq [c_{\mathrm{ZC}}^{p}[0]\, c_{\mathrm{ZC}}^{p}[1] \dots c_{\mathrm{ZC}}^{p}[K-1]]^{\mathsf{T}}$ with

$$c_{\mathrm{ZC}}^{p}[k] \triangleq e^{-j\pi\frac{p}{K}k(k+\mathrm{mod}(K,2))}, \quad k \in \mathcal{I}_K \tag{19}$$

and where $p \in \mathcal{I}_K$ the root index such that $\gcd(K,p) = 1$. We remark from (19) that ZC sequences are complex-valued which preserve coupling between timing and phase parameters. The impact of p on the performance is negligible for long sequences but shows a slight influence in severe FTN scenarios with short sequences. In the simulation setup described in Tab. I, it can be shown that $p = 31$ yields the lowest $\mathrm{CRB}(\xi|\boldsymbol{c}_{\mathrm{ZC}}^{p})$ at $\rho = 25/12$ [14]; it is thus the value chosen in the following.

In Fig. 4 we characterize the robustness of timing and phase estimation performance in presence of a residual normalized frequency offset (*i.e.*, $\nu \neq 0$). For $\boldsymbol{c} \in \{\tilde{\boldsymbol{c}}_{\psi,\mathrm{opt}}, \boldsymbol{c}_{\mathrm{ZC}}^{31}\}$, we depict $\mathrm{MSE}(\hat{\xi}_{\mathrm{ML}}(\boldsymbol{c}))$ and $\mathrm{MSE}(\hat{\phi}_{\mathrm{ML}}(\boldsymbol{c}))$ as a function of ν in Fig. 4a and Fig. 4b, respectively. The corresponding CRBs are also given as a reference.

First of all, ML-based estimators reach their corresponding CRBs at $\nu = 0$ for each pilot sequence and signaling density; this is also the case for shorter pilot sequences (*i.e.*, $K \geq 1$ at $E_s/N_0 = 10$ dB — not depicted here). For both timing and phase parameters $\mathrm{MSE}(\hat{\psi}_{\mathrm{ML}}(\boldsymbol{c}))$ quickly increases with

ν thereby requiring a prior coarse synchronization. An error floor is revealed at $\nu \geq 0.0055$; it characterizes the limits of GSS search interval previously chosen. By taking into account the pulse shape and the signaling density, the proposed pilot sequences $\tilde{\boldsymbol{c}}_{\psi,\mathrm{opt}}$ provide a significant performance gain compared to the reference ZC sequence $\boldsymbol{c}_{\mathrm{ZC}}^{31}$. This observation is particularly salient for the timing parameter. Our results encourage a density-specific pilot optimization in FTN scenarios.

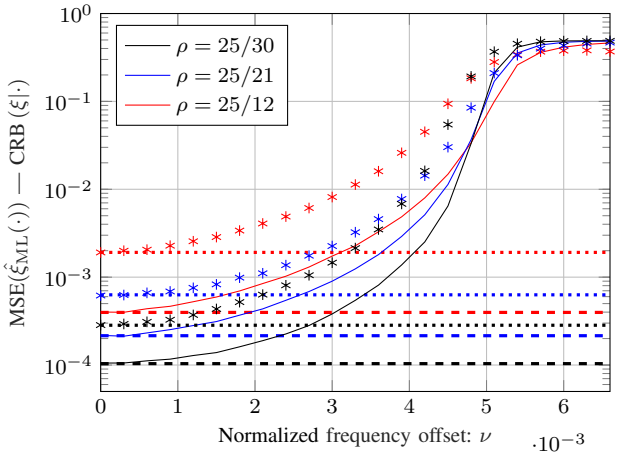

(a) Estimation of ξ *via* $\tilde{\boldsymbol{c}}_{\xi,\mathrm{opt}}$ and $\boldsymbol{c}_{\mathrm{ZC}}^{31}$ ($\phi = 0$)

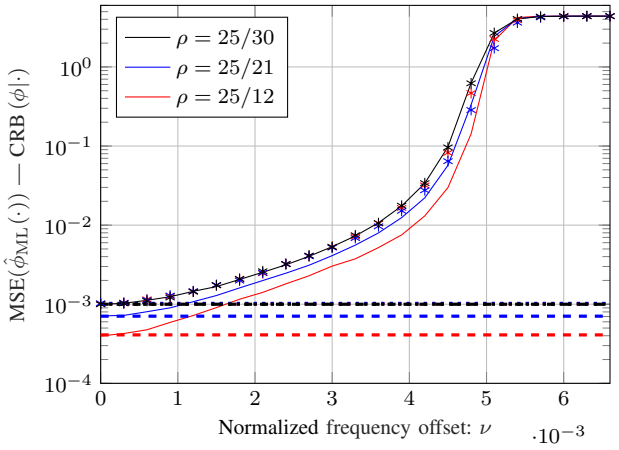

(b) Estimation of ϕ *via* $\tilde{\boldsymbol{c}}_{\phi,\mathrm{opt}}$ and $\boldsymbol{c}_{\mathrm{ZC}}^{31}$ ($\xi = 0$)

Fig. 4. $\mathrm{MSE}(\hat{\psi}_{\mathrm{ML}}|\tilde{\boldsymbol{c}}_{\psi,\mathrm{opt}})$ (solid lines) and $\mathrm{MSE}(\hat{\psi}_{\mathrm{ML}}|\boldsymbol{c}_{\mathrm{ZC}}^{31})$ (asterisk markers) as a function of the normalized frequency offset ν. Several transmission densities are considered: $\rho = 25/30$ (Nyquist) and $\rho \in \{25/21, 25/12\}$ (FTN). $\mathrm{CRB}(\psi|\tilde{\boldsymbol{c}}_{\psi,\mathrm{opt}})$ (dashed lines) and $\mathrm{CRB}(\psi|\boldsymbol{c}_{\mathrm{ZC}}^{31})$ (dotted lines) are displayed for comparison. All other parameters are set as in Tab. I.

V. Conclusion and Future Work

In the case of FTN singlecarrier systems, we studied the design of CRB-optimal pilot sequences in view of joint timing and phase estimation. To this extent we proposed closed-form approximations of the CRB suited for long enough sequences (*viz.*, more than 10 symbols). Using this result, optimal timing and phase pilots can be analytically determined *via* the signaling density and the pulse shaping function. The proposed optimal pilots revealed their superiority with respect to density-independent traditional ZC sequences. This observation is corroborated by ML estimators in presence of a residual frequency offset. Future work could include the design of FTN-specific non-data-aided frequency synchronization algorithms as a prerequisite to PA timing/phase estimation.

References

[1] J. E. Mazo, "Faster-than-Nyquist signaling," *Bell Syst. Tech. J.*, vol. 54, pp. 1451–1462, Oct 1975.

[2] G. Colavolpe, "Faster-than-Nyquist and beyond: How to improve spectral efficiency by accepting interference," in *IEEE Eur. Conf. and Exhib. on Optical Commun.*, Sep. 2011, pp. 1–25.

[3] A. Piemontese, A. Modenini, G. Colavolpe, and N. S. Alagha, "Improving the spectral efficiency of nonlinear satellite systems through time-frequency packing and advanced receiver processing," *IEEE Trans. Commun.*, vol. 61, no. 8, pp. 3404–3412, Aug. 2013.

[4] C. Le, M. Schellmann, M. Fuhrwerk, and J. Peissig, "On the practical benefits of faster-than-Nyquist signaling," in *IEEE Int. Conf. Adv. Technol. Commun.*, Oct. 2014, pp. 208–213.

[5] T. Delamotte, A. Knopp, and G. Bauch, "Faster-than-Nyquist signaling for satellite communications: A PAPR analysis," in *Int. ITG Conf. Syst., Commun. and Coding*, 2017, pp. 1–6.

[6] M. López Morales, D. Roque, and M. Benammar, "Timing estimation based on higher-order cyclostationarity for faster-than-Nyquist signals," *IEEE Commun. Letters*, vol. 23, no. 8, pp. 1373–1376, Jun. 2019.

[7] J. Wang, W. Tang, X. Li, and S. Li, "Filter hopping based faster-than-Nyquist signaling for physical layer security," *IEEE Wireless Commun. Lett.*, vol. 7, no. 6, pp. 894–897, Dec. 2018.

[8] Y. Li, J. Wang, W. Tang, X. Li, and S. Li, "A variable symbol duration based FTN signaling scheme for PLS," in *IEEE Int. Conf. on Wireless Commun. and Signal Process.*, Oct. 2019, pp. 1–5.

[9] A. Prlja and J. Anderson, "Reduced-complexity receivers for strongly narrowband intersymbol interference introduced by faster-than-Nyquist signaling," *IEEE Trans. Commun.*, vol. 60, no. 9, pp. 2591–2601, Sep. 2012.

[10] A. Modenini, F. Rusek, and G. Colavolpe, "Adaptive rate-maximizing channel-shortening for ISI channels," *IEEE Commun. Lett.*, vol. 19, no. 12, pp. 2090–2093, Dec. 2015.

[11] M. Kulhandjian, E. Bedeer, H. Kulhandjian, C. D'Amours, and H. Yanikomeroglu, "Low-complexity detection for faster-than-Nyquist signaling based on probabilistic data association," *IEEE Commun. Lett.*, vol. 24, no. 4, pp. 762–766, Dec. 2020.

[12] Y. Jiang, F.-W. Sun, and J. S. Baras, "On the performance limits of data-aided synchronization," *IEEE Trans. Inf. Theory*, no. 1, pp. 191–203, Jan. 2003.

[13] M. Morelli and A. A. D'Amico, "Maximum likelihood timing and carrier synchronization in burst-mode satellite transmissions," *EURASIP J. Wireless Commun. Netw.*, vol. 2007, pp. 1–8, Jun. 2007.

[14] L. Mounsif and D. Roque, "Optimal pilot sequences for timing estimation in faster-than-Nyquist systems," *IEEE Commun. Lett.*, vol. 25, no. 4, pp. 1236–1240, Apr. 2021.

[15] C. Shaw and M. Rice, "Optimum pilot sequences for data-aided synchronization," *IEEE Trans. Commun.*, vol. 61, no. 6, pp. 2546–2556, Jun. 2013.

[16] D. Chu, "Polyphase codes with good periodic correlation properties (corresp.)," *IEEE Trans. Inf. Theory*, vol. 18, no. 4, pp. 531–532, Jul. 1972.

[17] H. Meyr, M. Oerder, and A. Polydoros, "On sampling rate, analog prefiltering, and sufficient statistics for digital receivers," *IEEE Trans. Commun.*, vol. 42, no. 12, pp. 3208–3214, Dec. 1994.

[18] S. Kay, *Fundamentals of statistical signal processing, Volume I: Estimation theory*. Prentice Hall, Upper Saddle River, NJ, 1993.

[19] R. Gray, "On the asymptotic eigenvalue distribution of Toeplitz matrices," *IEEE Trans. Inf. Theory*, vol. 18, no. 6, pp. 725–730, 1972.

[20] T. K. Moon and W. C. Stirling, *Mathematical methods and algorithms for signal processing*. Prentice Hall, Upper Saddle River, NJ, 2000.

[21] J. Kiefer, "Sequential minimax search for a maximum," *Proc. Amer. Math. Soc.*, vol. 4, no. 3, pp. 502–506, Jun. 1953.